A Computer Modeling Study of Perfect and Defective Silver (111) Surfaces

N. H. de Leeuw*,†,‡, and C. J. Nelson†,§

School of Crystallography, Birkbeck College, University of London, Malet Street, London WC1E 7HX, U.K., Department of Chemistry, University College, University of London, 20 Gordon Street, London WC1H 0AJ, U.K., and Davy Faraday Research Laboratory, Royal Institution of Great Britain, Albemarle Street, London W1X 4BS, U.K.

Received: September 16, 2002; In Final Form: January 20, 2003

Density functional theory calculations of the ideal and defective (111) surfaces of silver have shown that although the perfect surface shows very little atomic relaxation the introduction of vacancies, adatoms, and step edges on the surface leads to significant bond distortions in the near-defect regions. The defective surfaces are not significantly less stable than the perfect (111) surface and the average calculated surface energy of 0.49 eV per surface atom agrees well with the experimental value of 0.55 eV/atom. Electron density contour plots show delocalization along the surface compared to the bulk metal, while a more gradual decline of the electron density in the defect areas compared to the perfect surface leads to a more level electronic structure of the defective surfaces than their atomic structure. The formation energies of surface vacancies and adatoms with respect to gaseous silver atoms are +3.20 eV and −2.03 eV, respectively, while the introduction of a step edge on the surface costs 0.42 eV per edge atom with respect to the planar surface. Adsorption of an adatom at the step edge releases 2.50 eV and the lower-coordinated edge sites, rather than the terrace sites of the planar (111) surface, are thus energetically preferred sites for further silver growth. Segregation of vacancies from the bulk material to the (111) surface is calculated to be exothermic at −0.18 eV per vacancy and recombination of a surface vacancy with a surface adatom will release 1.81 eV per vacancy/adatom pair.

Introduction

Silver metal is of considerable industrial importance as a catalytic material, for example, in the selective partial oxidation of ethene to its epoxide, which is a widely used precursor for a host of chemical products.[1,2] As a consequence of its catalytic significance and also because of the ease with which silver is investigated using surface science techniques such as scanning tunneling microscopy (STM), e.g., refs 3 and 4, silver surfaces have been the subject of much research, both experimentally, e.g., refs 5−8, and theoretically, e.g., refs 9−14. Often, the reactivity of the metal is probed by the adsorption of small molecules, e.g., NO,[15,16] CO_2,[17] or SiO and SiS,[18] while a variety of experimental techniques has been used to study the interactions of silver with a host of small organic adsorbates, such as methanol,[19] phenol,[20] *tert*-butyl nitrite,[21] and sulfur-containing compounds.[22−24] More recently, experimental techniques have been employed to study the synthesis and behavior of silver nanoparticles, e.g., refs 25 and 26.

As oxygen plays a crucial role in the catalytic epoxidation process, e.g., refs 27 and 28, its presence and behavior at the silver surface has been studied by a number of groups, often as the main species under investigation, for example, the STM study by Carlisle and King of the formation of an oxide film at the silver (111) surface,[29] the effects of oxygen on silver morphology[30,31] or the theoretical studies of oxygen adsorption by Li et al.[32] and Wang et al.,[33] and oxygen dissociation on Ag (110) surfaces by Salazar et al.,[34] but also as a coadsorbate, e.g., the spectroscopic study of ethene and ethene oxide adsorption on an oxygen-covered Ag(111) surface by Stacchiola et al.[35] and the computational studies by Avdeev and Zhidomirov[36] and Sun et al.[37] of the adsorption of ethene and methanol, respectively, on oxidized silver surfaces.

However, the bare silver metal is often not very selective in the catalytic partial oxidation processes, but after exposure to and subsequent adsorption of chlorine the metal is observed to demonstrate a significantly increased selectivity toward the desired reaction product, e.g., ref 38. As a result, the interaction of halogens or halide-containing adsorbates with silver surfaces has been studied both experimentally, for example, by the use of scanning tunneling microscopy,[39] temperature-programmed desorption,[40] a range of spectroscopic techniques,[41] and computationally.[42−44]

Clearly, if we are to understand the catalytic and adsorptive behavior of silver, we need to understand the surface structures and reactivities of this material and investigate these processes at the atomic level. In this work, we have employed electronic structure calculations based on the density functional theory within the generalized gradient approximation to investigate and compare the geometry and electronic structure of the perfect and three defective (111) surfaces of silver metal—one surface consisting of a series of (111) terraces offset from each other by monatomic steps, and two (111) planes which are partially vacant in silver atoms. In addition, initial processes of surface growth and vacancy segregation were studied and are discussed in the light of experimentally observed surface diffusion.

Theoretical Methods

The total energy and structure of the silver surfaces were determined using the Vienna Ab Initio Simulation Program (VASP),[45] which is an established Density Functional Theory

* Corresponding author. E-mail: n.deleeuw@mail.cryst.bbk.ac.uk.
† School of Crystallography, Birkbeck College, University of London.
‡ Department of Chemistry, University College, University of London.
§ Davy Faraday Research Laboratory, Royal Institution of Great Britain.

10.1021/jp027001t CCC: $25.00
Published on Web 03/22/2003

TABLE 1: Calculated and Experimental Cohesive Energies and Bulk Moduli of Silver

method	$E_{cohesive}$ (eV atom^{-1})	B ($\times 10^{11}$ Nm^{-2})
LDA	3.707	1.305
GGA	2.650	1.040
experiment	2.950	1.007

(DFT) simulation package, employing plane waves for the valence electrons and ultra-soft pseudo-potentials for the effective interaction of the valence electrons with the atomic cores.[46] This methodology is now well established and has been successfully applied to the study of metals, e.g., ref 47, semiconductors, e.g., ref 48, and ionic materials, e.g., ref 49. In our calculations the core consisted of orbitals up to and including the 3d orbital for Ag, leaving the 4d and 5s electrons to be treated explicitly. Although previous studies of the perfect silver (111) surface[50] and surface vacancy formation[51] were executed using the Local Density Approximation (LDA), the calculations in this study were performed within the generalized-gradient approximation (GGA), using the exchange-correlation potential developed by Perdew and Wang,[52] rather than LDA. Although the GGA approach has been shown to give reliable results for a range of metals and ionic materials, e.g., refs 44 and 53, we have nevertheless compared the two methods for silver metal by calculating the cohesive energy and bulk modulus (eq 1):

$$B = \frac{-\Delta P}{(\Delta V/V)} \tag{1}$$

where ΔP is the change in pressure corresponding to the change in volume ΔV. The experimental[54] and calculated values are shown in Table 1, from which it is clear that for these properties GGA gives better agreement with experiment than LDA. As we are interested in investigating the energetics of adsorption and growth of silver at different surface sites, good agreement with experimental binding energies is essential if our calculations are to be reliable.

For surface calculations, where two energies are compared, it is important that the total energies are well converged. The degree of convergence depends on a number of factors, two of which are the plane-wave cutoff and the density of k-point sampling within the Brillouin zone. We have, by means of a series of test calculations on bulk silver, determined values for E_{cut} (300 eV) and the size of the Monkhorst-Pack k-point mesh[55] ($11 \times 11 \times 11$). In addition, we checked the convergence of the total energy for the slab calculations and found that the most suitable value of E_{cut} is the same as for the bulk material.

The optimization of the atomic coordinates (and unit cell size/shape for the bulk material) was performed via a conjugate gradients technique which utilizes the total energy and the Hellmann−Feynman forces on the atoms (and stresses on the unit cell). We used the usual approach for modeling the surfaces, using three-dimensional periodic boundary conditions by considering slabs of Ag. In addition to the k-point density and E_{cut} discussed above, the convergence in surface calculations is also dependent on the thickness of the slab of material and the width of the vacuum layer between the slabs. Again, we checked convergence by running a series of test calculations with different slab thicknesses and gap widths. These calculations showed that although a nine-layer slab will give the most accurate results, the surface energy has converged to within 0.01 J m^{-2} at five layers thickness. In addition, we found that it was sufficient if in each calculation the vacuum layer was at least 16 Å between the images of the surfaces either side of the void. The Methfessel-Paxton method[56] with a smearing width of 0.20 eV was chosen for the determination of the partial occupancies, which method gives a very accurate description of the total energy of the system and is especially suitable for large supercells.

Results and Discussion

Silver has a face-centered cubic structure, where in the bulk each silver atom is twelve-coordinated. The experimental lattice parameters of silver are $a = b = c = 4.101$,[54] which upon full electronic geometry optimization expanded somewhat to $a = b = c = 4.161$, although still in excellent agreement with experiment (~1.5%). The most stable silver surface is the (111) surface, which is a hexagonal close-packed plane of silver atoms, e.g., ref 57. One measure of the stability of the surface is the surface energy, which is calculated as follows:

$$\gamma = \frac{U_S - U_B}{A} \tag{2}$$

where U_S is the energy of the slab of silver containing the surfaces, U_B is the energy of an equivalent number of bulk silver atoms, and A is the surface area. The surface energy of a particular surface is thus a measure of the energy required to cleave the bulk crystal, exposing the surface, where a small, positive value for the surface energy indicates a stable surface.

Planar (111) Surface. We first investigated the structural and electronic character of the ideal, defect-free (111) surface, which is shown in Figure 1. The electron density contour plots, shown in this figure in a plane through the silver atoms in the first, fourth, and seventh layers from the top surface, show a large degree of localization of the electron density around the individual silver atoms in the bulk, although with some density distributed along Ag−Ag bonds. The electron density at the surface is far more delocalized over the surface silver atoms. The surface energy (Table 2) was calculated at 0.72 J m^{-2} or 0.34 eV/surface atom, which agrees well with previous theoretical studies, e.g., 0.36 eV/atom[57] or 0.46 eV/atom,[44] but is lower than the experimental value of 0.55 eV/atom.[58] As could be expected from the low value of the surface energy, the ideal (111) surface shows negligible structural relaxation with practically bulk termination of the two identical surfaces at either end of the slab. The interlayer spacing between the first two surface layers has contracted by about 1.4% of the bulk interlayer spacing which is in very good agreement with experimentally found contractions of <2% [59] or 2.5%[60] and previous calculations of 0.3% to 1.4%.[57] The interatomic Ag−Ag distances in the surface layers are also approximately 1.5% shorter than those in the bulk material (Figure 1). The second interlayer distance is also contracted, but only by less than 0.3%, in contrast with some experimental and theoretical findings where this spacing is found to be dilated by 0.6%[60] and 0.04%, respectively.[57] However, other computational studies do predict a contraction of this second interlayer spacing by 0.07%[57] or alternatively an absence of any dilation or contraction,[61] while a recent LEED study showed both first and second layers to contract by $0.5 \pm 0.3\%$ and $0.4 \pm 0.4\%$, respectively, at 128 K.[62] In any case, the dilation/contraction of this second interlayer spacing is very small and theory and experiment all agree to within about 1%, which is well within the limits of accuracy for either method.

Defective (111) Surfaces. As experimental surfaces are never perfect and catalytic processes often occur at surface defects,

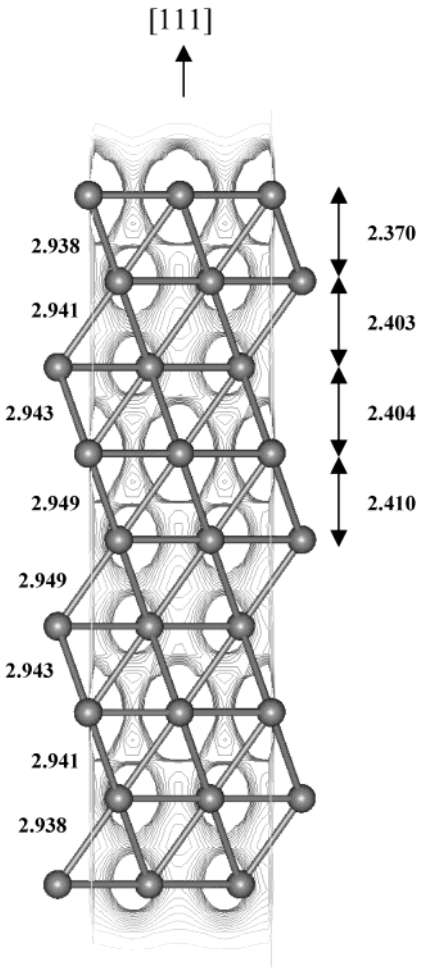

Figure 1. Side view of the relaxed nine-layer silver slab with (111) surfaces at either end, showing both interatomic and interlayer spacings (in Å) and electron density contour plots through the silver atoms of the 1st, 4th, and 7th layers from the top, contour levels are from 0.02 to 0.30 e/Å^3 at 0.02 e/Å^3 intervals. (The apparent shift of electron density away from the atoms in the other layers is due to the fact that the electron density plane shown is not centered upon those atoms and hence shows electron density in a plane away from the atomic centers).

TABLE 2: Surface Energies of the Ideal and Defective Silver Surfaces

(111) surface	γ (J m^{-2})	γ (eV/atom)
ideal planar	0.72	0.34
stepped	0.81	0.48
11% vacancies	0.86	0.45
11% adatoms	0.88	0.53

such as vacancies, steps, and growth islands, we also investigated three defective (111) surfaces. We first studied a 3 × 3 surface supercell, where one of the nine surface atoms had been removed from each (111) surface at either end of the slab, which left the two surfaces with an 11% concentration of isolated surface vacancies. In addition to a partially vacant surface, we also investigated the effect of isolated silver atoms added to the surface. Again we studied a 3 × 3 surface supercell, this time with an 11% coverage of isolated silver atoms on the two planes. Finally, we studied a stepped (111) surface to investigate how the electronic structure and stability of the surface is affected by the presence of an extended step edge of low-coordinated surface atoms instead of isolated point defects. Unlike the surface vacancies and adatom calculations above, the steps on the (111) surface were not formed from defects on the 3 × 3 planar supercell, as this would lead to a surface containing either one missing row of silver atoms or two missing rows (i.e., identical to a row of adatoms), which would not be a realistic model for a stepped surface. The stepped surface (shown in Figure 2) was therefore created by adjusting the lattice vectors of the supercell to form a repeating slab, where the repeat unit was offset by one atomic layer with respect to the first cell. As a result the simulation cell has a true step at the surface, which is repeated from cell to cell, with a terrace of three silver atoms deep between the steps. This method of creating stepped planes, which has been successfully employed in previous simulations of stepped calcite and forsterite surfaces, e.g., ref 63, avoids the occurrence of two opposing steps in a single simulation cell, which would lead to a crenellated rather than a truly stepped surface.

From the surface energies in Table 2, we see that the introduction of surface defects has a destabilizing effect compared to the ideal (111) surface, although the change in surface energies per unit area at 12.5−22% from the perfect surface is not excessive. There is little difference between the surface energies of the three defective surfaces, although the extended surface defect in the form of a low-coordinated step has the least destabilizing effect. The introduction of isolated adatoms creates a rougher surface than the introduction of vacancies, which effect is shown in their relative stabilities. The relatively small increase in surface energy per unit area upon introduction of the three types of surface defects indicates that we may expect all these defects to be present on an experimental (111) surface and they should therefore be taken into account when studying, for example, surface reactivities. When we compare the surface energies per surface atom of the defective surfaces, at 0.48 eV/atom (step), 0.45 eV/atom (vacancy), and 0.53 eV/atom (adatom) with the experimental surface energy of the (111) surface of 0.55 eV/atom,[55] we see that they are now much closer to the experimental value. "Real" (111) surfaces will contain a mixture of the surface defects modeled in this work and the experimental surface energy of 0.55 eV/atom agrees much better with the average of the calculated surface energies of 0.49 eV/atom, containing all three defects in addition to the perfect (111) surface atoms, even though experimental surfaces will not of course contain these defects in equal proportions. However, these calculations do show that inclusion of surface defects in surface energy calculations gives a more reasonable value for the surface energy compared to experiment.

Stepped (111) Surface. Figure 2 shows the stepped (111) surface with electron density contour plots through the silver atom at the step edge. The Ag−Ag bond distances along the step edge are all 2.94 Å, but the bond lengths between the silver atoms at the edge and those on the terraces behind and below are considerably shorter at 2.89 to 2.91 Å. In addition, the distance to the silver atoms in the second layer below the edge atom has shortened by about 3% from its bulk value to 2.86 Å. As a result of these shortened bonds the silver atoms at the step edge are pulled into the surface, hence flattening the step edge. We can see from the electron density contour plots that the electron density distribution is delocalized over the step in a fashion similar to that in the perfect surface shown in Figure 1. In the step region, the delocalized electron density is smoothly distributed over the hollow below the step, with the contour levels around the atom in the kink site spaced more widely apart than around the atoms on the terraces and on the perfect surface. As a result the electronic structure of the stepped surface is much more level than the geometry of the step would suggest. However, compared to a coordination number of 12 for silver

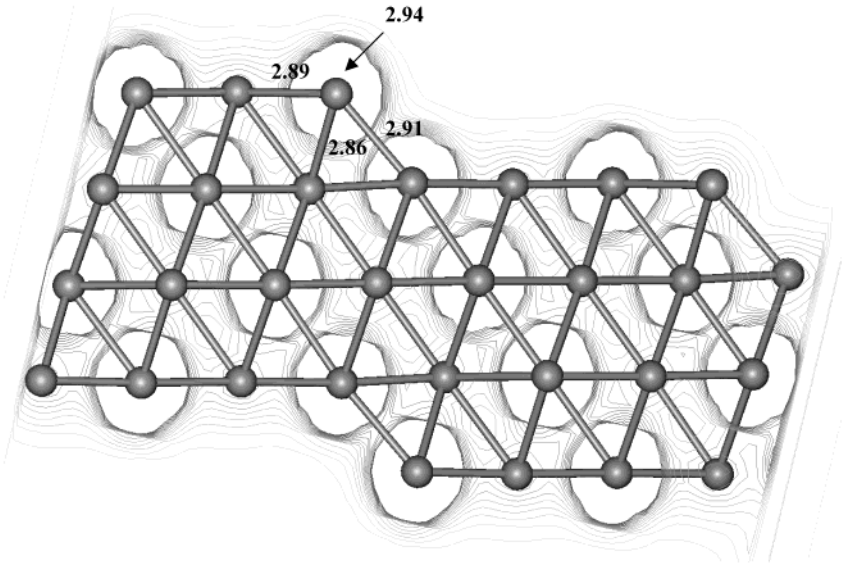

Figure 2. Side view of the fully optimized structure of the stepped (111) surface, showing interatomic spacings (in Å) and electron density contour plots through silver atoms on the step edge (contour levels are from 0.02 to 0.30 e/Å^3 at 0.02 e/Å^3 intervals).

atoms in the bulk metal, the silver atoms in the planar (111) surface are coordinated to nine others—six in the plane and three to the layer below, but the atoms on the step edge are coordinated to only seven others. We would therefore expect these edge atoms to be more reactive than the silver atoms on the terraces toward, for instance, adsorbates in an attempt to increase their coordination. If we look at the surface energies per surface atom, we see that not only is the surface energy of the stepped surface with respect to the bulk metal higher than that of the perfect (111) surface (0.48 eV/atom compared to 0.34), but the formation energy of the step compared to the perfect surface is even more significant at 0.42 eV per step atom formed (calculated as the difference between the energy of the planar surface per atom and the correspondening energy of the stepped surface per step atom). Hence, in addition to the low coordination and therefore probably higher reactivity of the atoms at the step edge, there is also an energetic incentive for annihilation of the step edge, which we therefore consider to be a prime site for further silver growth to occur, for example, by vapor deposition or surface diffusion of silver atoms toward the step edge. To test the hypothesis that further silver atoms would preferentially attach at the stepped site, we also calculated the addition of a silver atom both at the step edge and as an adatom on the perfect (111) surface.

(111) Surface with Silver Adatom. Figure 3 shows the (111) surface with an adatom leading to a surface partially covered with 11% isolated adatoms. The electron density contour plots show the same effect as on the stepped surface, where the contours are spaced more widely apart in the region immediately surrounding the adatom, hence smoothing the electronic structure of the region around the defect and neutralizing to a certain extent the kink sites introduced on the surface by the adsorption of the adatom. We calculated the energy of formation of the adatom both with respect to gaseous silver atoms and with respect to bulk silver metal as follows:

$$\text{perfect surface} + \text{Ag} \rightarrow \text{surface with adatom} \qquad (3)$$

where Ag is either an atom in bulk silver or in the gaseous state. Calculating the defect formation energies with respect to bulk silver enables us to compare our calculations with previous work whereas calculating it with respect to gaseous silver

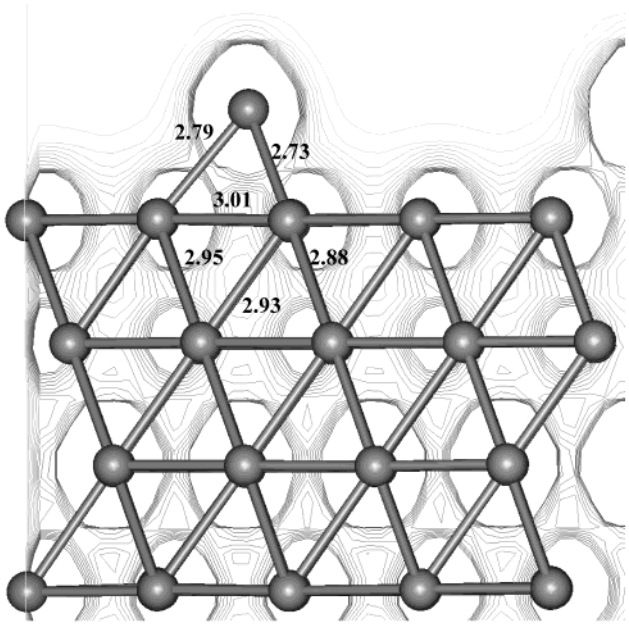

Figure 3. Side view of the relaxed (111) surface covered by 11% adatoms, showing some interatomic spacings (in Å) and electron density contour plots through the silver adatoms (contour levels are from 0.02 to 0.30 e/Å^3 at 0.02 e/Å^3 intervals).

enables us to evaluate the defect formation with respect to the cohesive energy of the silver metal and to test the nonlinearity of metal bond formation energies for silver. When compared with silver in the bulk metal, the formation energy of the adatom at the surface is 0.62 eV/atom. Haftel calculated a formation energy of an adatom at the silver (111) surface of 0.85 eV/atom,[64] which is somewhat more than our calculated formation energy. The discrepancy may be due to the fact that Haftel used potential-based methods for his calculations which do not include electronic polarizability to the same extent, but it may also be influenced by the necessarily smaller size of our simulation cells due to the computationally expensive electronic structure methods used in this work. Haftel does not give the reference state for his formation energy but as it is positive, we presume that it is calculated with respect to bulk metal rather than gaseous silver atoms.

We calculated that 2.03 eV is released upon adsorption of a gaseous silver atom at the perfect surface. As the adatom forms three bonds to surface atoms, which as a result also increase their coordination by one, the total Ag coordination number is increased by six through the adsorption of the adatom. The cohesive energy of 2.65 eV per Ag atom listed in Table 1 is released upon the formation of the silver lattice out of gaseous silver atoms, where each silver atom becomes coordinated to 12 nearest neighbors, i.e., an average of 0.22 eV per Ag−Ag bond per silver atom involved in the bonding (0.44 eV per bond). Hence, if the cohesive energy were to be bond additive, the formation of three bonds should release 1.32 eV. However, we found that an extra 0.71 eV (68.0 kJ mol^{-1}) is released, a clear example of the fact that the energy of bond formation in silver metal is not linear. The enhanced exothermicity of the adatom adsorption compared to the averaged cohesive energy is due to a combination of close coordination of the adatom to the surface and localized relaxation of the surface in the region surrounding the defect. For example, the bond distances listed in Figure 3 show that the Ag−Ag bond lengths between adatom and surface atoms are very small at 2.73−2.79 Å, a decrease of 5−7% from the bulk value, although the bonds lying in the surface have lengthened somewhat (by about 2%) to accommodate the close coordination of the adatom to the surface. However, to accommodate this bond lengthening parallel to the surface, the bond lengths to the second layer have decreased again in turn (by up to 2.5%).

When isolated adatoms are adsorbed at the step edges, 2.50 eV/adatom is released with respect to gaseous silver atoms and the energy required with respect to bulk silver metal is 0.15 eV/adatom. The step edge is clearly an energetically more advantageous site for silver growth than attachment to the planar terraces. However, although adsorption of the adatom at the step edge is more exothermic than on the terrace (by 0.47 eV/adatom), the extra energy released beyond the averaged cohesive energy is less at the step edge than on the planar surface discussed above, only 0.30 eV more per adatom than the average energy per Ag−Ag bond and the stability of the stepped surface containing isolated adatoms has decreased. Whereas the surface energy of the stepped surface was 0.81 J m^{-1}, adsorption of adatoms at the step leading to a crenellated step edge increases the surface energy to 0.85 J m^{-1}. The decrease in stabilitity is caused by the presence of the step, which hinders the same extensive relaxation of the area surrounding the defect, which we saw around the adatom on the planar surface. For example, the adatom becomes coordinated to a total of five atoms (compared to three on the planar terrace described above), two on the step edge at 2.87 Å, one on the terrace below, and two kink site atoms in the hollow between step and terrace below at 2.79 Å, but whereas the Ag−Ag bonds between terrace and adatom were shortened by up to 7% on the planar surface with respect to the bulk value, we see only shortening of the bonds between the adatom and the silver atoms at the edge and on the terrace of up to 5% compared to the bulk, which is moreover only a decrease of 2% with respect to the stepped surface before adsorption of the adatom. Hence, if we compare the adsorption of the adatom at the planar surface, with the formation of three short Ag−Ag bonds, with that at the stepped surface, forming five longer Ag−Ag bonds, we see that the energy released gets less as more bonds are formed, from an average of 0.68 eV per Ag−Ag bond per Ag atom for 3-fold coordination through an average of 0.50 eV per Ag−Ag bond per Ag atom for 5-fold coordination to 0.22 eV per Ag−Ag bond per Ag atom in the perfect 12-coordinated lattice.

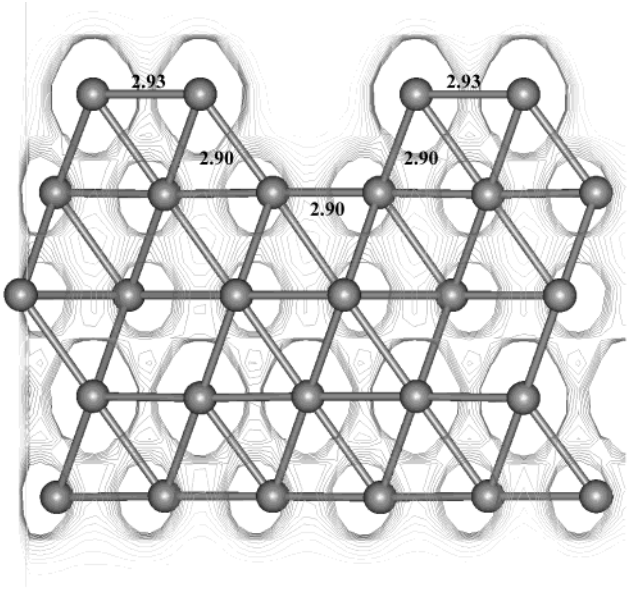

Figure 4. Side view of a slice containing the vacancy of the relaxed 11% vacant (111) surface, showing interatomic spacings (in Å) and electron density contour plots through the silver vacancy (contour levels are from 0.02 to 0.30 e/$Å^3$ at 0.02 e/$Å^3$ intervals).

Surface and Bulk Vacancies. We next calculated the structure and energetics of the formation of surface vacancies. Figure 4 shows the partially vacant (111) surface with the electron density contour plots through the plane of the surface vacancy. We see that again the electron density contours in the vacancy area are spaced much more widely apart than between the surface atoms, which lessens the effect of the vacancy on the electronic structure of the (defective) surface. The formation of vacancies is less energetically expensive than the adsorption of surface adatoms, costing 0.55 eV/vacancy with respect to the bulk metal. Haftler[64] quotes a vacancy formation energy on the (111) surface of 0.76 eV/vacancy which is again slightly higher than our formation energy (0.55 eV), in line with the adatom formation energies. Again, our vacancy formation energy may be less than his calculated energy because of the extensive electronic relaxation we saw in Figure 4, which cannot be modeled accurately using potential-based methods. For a system in which there is no atomic or electronic relaxation on vacancy formation, the vacancy energy should be close to twice the cohesive energy of the metal. When the vacancy is formed the desorbed atom has lost coordination to its nine nearest neighbors, while the coordination of nine silver atoms around the vacancy is also lessened by one. Similar to the adatom above, we see that again the energy necessary to create the vacancy at 3.20 eV with respect to a gaseous silver atom is considerably less (by 0.78 eV/vacancy) than a linear summation of the average cohesive energy per bond, which would amount to 3.98 eV. As is shown in Figure 4, all Ag−Ag bonds surrounding the vacancy have shortened (1.0−1.7%), in effect making the vacancy shallower, which in conjunction with the electronic relaxation mentioned above reduces the formation energy of the vacancy compared to the cohesive energy. We also modeled the formation of vacancies in the bulk metal, where the simulation cell consisted of the same 3×3 supercell as for the surface calculations, but without the vacuum gap between the surface slabs. We calculated that vacancy formation in the bulk costs 3.38 eV/vacancy with respect to the gaseous atom. It is clear that vacancy formation in the bulk material is energetically more expensive than at the surface and we can hence calculate

the energy of segregation of the vacancy from surface to bulk as follows:

$$Ag_{(surface)} + V_{(bulk)} \rightarrow Ag_{(bulk)} + V_{(surface)} \quad (4)$$

The calculated segregation energy is −0.18 eV/vacancy (−17.1 kJ mol^{-1}), which indicates that there is an energetic incentive for the vacancy to segregate to the surface. In addition, we can calculate the process whereby a surface vacancy and a surface adatom combine to form the perfect (111) surface. This process is calculated to release 1.81 eV per adatom/vacancy pair (174 kJ mol^{-1}), from the combination of a vacancy and an adatom into the perfect (111) surface, and there is thus a large energetic incentive for these two defects to be mutually annihilated, although this will of course also depend on the ease of surface diffusion of either species. Diffusion of both adatoms and vacancies on the silver (111) surface has, however, been observed to proceed rapidly by a number of groups using scanning tunneling microscopy techniques, e.g., ref 65, and from the calculated energy for vacancy/adatom pair combination we may therefore expect that this process will indeed occur on the real surface.

Conclusion

We have executed a series of electronic structure calculations, based on the density functional theory within the generalized gradient approximation, of the ideal and three defective (111) surfaces of silver. The perfect surface shows very little atomic relaxation of the surface atoms with respect to the bulk metal, in line with experimental findings, although the electron density is more delocalized along the surface compared to the bulk. On the defective surfaces, the electron density is distributed in such a way as to minimize the effect of the defect, e.g., smoothening the step and adatom edges and filling in the vacancy, through a more gradual decline of electron density in the defect areas than is observed at the perfect surface.

Atomic relaxation of the surface areas surrounding the defects also plays a role in stabilizing the defective surface, especially shortening of the Ag−Ag bonds in the immediate defect region. The energies released upon adsorption of the adatoms are larger than the bond average from the cohesive energy, while the energy expended upon formation of the vacancies is less than the equivalent average energy per broken bond. Our calculations are thus a clear example that the cohesive energy of a metal is not bond additive. Although the defective surfaces are destabilized by the presence of the defect compared to the perfect (111) surface, the calculated surface energies of the defective surfaces are not significantly higher and we would hence expect these surface defects to be observed on real surfaces. An average of the surface energies of the combined defective surfaces, containing perfect terraces as well as steps, adatoms, and surface vacancies, agrees well with the experimental surface energy and shows that the inclusion of surface defects in surface energy calculations gives surface energies which are closer to experimentally determined values than those based on the perfect surface alone.

The segregation of silver vacancies from the bulk metal to the (111) surface is calculated to be an exothermic process. Rapid surface diffusion of vacancies and adatoms has been observed on the experimental silver (111) surface, and as the recombination of surface vacancies with surface adatoms is calculated to be highly exothermic we would predict that this process will occur to a significant extent on the real silver (111) surface. Similarly, as the preferred site for adatoms is at the step edges rather than adsorbed onto the terraces, we would also expect surface diffusion of adatoms to edge sites to occur, which process is calculated to release 45 kJ mol^{-1} for each adatom. As the recombination of an adatom with a surface vacancy releases 174 kJ mol^{-1} this is obviously the preferred process, but in the absence of suitable surface vacancies, the energetic incentive of diffusion toward edge sites may well be significant in surface diffusion of isolated adatoms. Moreover, as the creation of a step at the surface costs only 40 kJ mol^{-1} per edge atom, clustering of isolated adatoms into islands will also be an exothermic process.

Future work will include employing classical molecular dynamics simulations to investigate surface diffusion of atoms and vacancies and further electronic structure calculations to investigate relative reactivities of the various surface sites discussed in this work by way of adsorption of small molecules such as chlorine.

Acknowledgment. C.J.N. thanks Drs. M. Alfredsson and B. Slater and Professor C. R. A. Catlow for useful discussions and the EPSRC for a studentship. N.H.dL. thanks the Engineering and Physical Sciences Research Council for an Advanced Research Fellowship and acknowledges the Royal Society Grant No. 22292 for funding and the Materials Chemistry and Mineral Physics Consortia for provision of computational facilities on the Cray T3E high-performance computing system.

References and Notes

(1) Serafin, J. G.; Liu, A. C.; Seyermonir, S. R. *J. Mol. Catal. A* **1998**, *131*, 157.
(2) Bukhtiyaros, V. I.; Prosvirin, I. P.; Kvon, R. I.; Goncharova, S. N.; Bal'zhinimaev, B. S. *J. Chem. Soc., Faraday Trans.* **1997**, *93*, 2323.
(3) Koch, R.; Sturmat, M.; Schulz, J. J. *Surf. Sci.* **2000**, *454*, 543.
(4) Kagami, S.; Minoda, H.; Yamamoto, N. *Surf. Sci.* **2001**, *493*, 78.
(5) Bremer, J.; Hansen, J.-K.; Stahrenberg, K.; Worren, T. *Surf. Sci.* **2000**, *459*, 39.
(6) Degroote, B.; Dekoster, J.; Langouche, G. *Surf. Sci.* **2000**, *452*, 172.
(7) Puygranier, B. A. F.; Dawson, P.; Lacroute, Y.; Goudonnet, J.-P. *Surf. Sci.* **2001**, *490*, 85.
(8) Oshima, Y.; Nakade, H.; Shigeki, S.; Hirayama, H.; Takayanagi, K. *Surf. Sci.* **2001**, *493*, 366.
(9) Yu, B. D.; Scheffler, M. *Phys. Rev. Lett.* **1996**, *77*, 1095.
(10) Longo, R. C.; Rey, C.; Gallego, L. J. *Surf. Sci.* **2000**, *459*, L441.
(11) Baletto, F.; Mottet, C.; Ferrando, R. *Phys. Rev. Lett.* **2000**, *84*, 5544.
(12) Zhao, S. J.; Wang, S. Q.; Yang, Z. Q.; Ye, H. Q. *J. Phys.: Condens. Matter* **2001**, *13*, 8061.
(13) Baletto, F.; Ferrando, R. *Surf. Sci.* **2001**, *490*, 361.
(14) Narasimhan, S. *Surf. Sci.* **2002**, *496*, 331.
(15) Itoyama, T.; Wilde, M.; Matsumoto, M.; Okano, T.; Fukutani, K. *Surf. Sci.* **2001**, *493*, 84.
(16) Guo, X.-C.; Madix, R. J. *Surf. Sci.* **2002**, *496*, 39.
(17) Guo, X.-C.; Madix, R. J. *Surf. Sci.* **2001**, *489*, 37.
(18) Alikhani, M. E. *J. Chem. Soc., Faraday Trans.* **1997**, *93*, 3305.
(19) Nagy, A. J.; Mestl, G.; Rühle, T.; Weinberg, G.; R. Schlögl, R. *J. Catal.* **1998**, *179*, 548.
(20) Lee, J.; Ryu, S.; Kim, S. K. *Surf. Sci.* **2001**, *481*, 163.
(21) Lee, I.; Kim, S. K.; Zhao, W.; White, J. M. *Surf. Sci.* **2002**, *499*, 41.
(22) Compagnini, G.; De Bonis, A.; Cataliotti, R. S.; Marletta, G. *Phys. Chem. Chem. Phys.* **2000**, *2*, 5298.
(23) Zharnikov, M.; Frey, S.; Rong, H.; Yang, Y.-J.; Heister, K.; Buck, M.; Grunze, M. *Phys. Chem. Chem. Phys.* **2000**, *2*, 3359.
(24) Kondoh, H.; Tsukabayashi, H.; Yokoyama, T.; Ohta, T. *Surf. Sci.* **2001**, *489*, 20.
(25) Peyser, L. A.; Lee, T. H.; Dickson, R. M. *J. Phys. Chem. B* **2002**, *106*, 7725.
(26) Kamat, P. V. *J. Phys. Chem. B* **2002**, *106*, 7729.
(27) Bertole, C. J.; Mims, C. A. *J. Catal.* **1999**, *184*, 224.
(28) Nagy, A. J.; Mestl, G.; Schlögl, R. *J. Catal.* **1999**, *188*, 56.
(29) Carlisle, C. I.; King, D. A. *Phys. Rev. Lett.* **2000**, *84*, 3899.
(30) Nagy, A. J.; Mestl, G.; Herein, D.; Weinberg, G.; Kitzelmann, E.; Schlögl, R. *J. Catal.* **1999**, *182*, 417.
(31) Millar, G. J.; Nelson, M. L.; Uwins, P. J. R. *J. Chem. Soc., Faraday Trans.* **1998**, *94*, 2015.

(32) Li, W.-X.; Stampfl, C.; Scheffler, M. *Phys. Rev. B* **2002**, *65*, 075407.
(33) Wang, Y.; Jia, L. L.; Wang, W. N.; Fan, K. N. *J. Phys. Chem. B* **2002**, *106*, 3662.
(34) Salazar, M. R.; Kress, J. D.; Redondo, A. *Surf. Sci*. **2000**, *469*, 80.
(35) Stacchiola, D.; Wu, G.; Kaltchev, M.; Tysoe, W. T. *Surf. Sci*. **2001**, *486*, 9.
(36) Avdeev, V. I.; Zhidomirov, G. M. *Surf. Sci*. **2001**, *492*, 137.
(37) Sun, Q.; Wang, Y.; Fan, K.; Deng, J. *Surf. Sci*. **2000**, *459*, 213.
(38) Hawker, S.; Mukoid, C.; Badyal, J. P. S.; Lambert, R. M. *Surf. Sci*. **1989**, *219*, L615.
(39) Frank, E. R.; Hamers, R. J. *J. Catal*. **1997**, *172*, 406.
(40) Wu, G.; Stacchiola, D.; Kaltchev, M.; Tysoe, W. T. *Surf. Sci*. **2000**, *463*, 81.
(41) Endo, O.; Kondoh, H.; Yonamoto, Y.; Staicu-Casagrande, E. M.; Lacombe, S.; Guillemot, L.; Esaulov, V. A.; Pasquali, L.; Nannarone, S.; Canepa, M. *Surf. Sci*. **2001**, *480*, L411.
(42) Shen, B.; Fang, Z.; Fan, K.; Deng, J. *Surf. Sci*. **2000**, *459*, 206.
(43) Wang, Y.; Wang, W.; Fan, K.; Deng, J. *Surf. Sci*. **2001**, *487*, 77.
(44) Doll, K.; Harrison, N. M. *Phys. Rev. B* **2001**, *63*, 165410.
(45) Kresse, G.; Hafner, J. *Phys. Rev. B* **1993**, *47*, 5858; Kresse, G.; Hafner, J. *Phys. Rev. B* **1994**, *49*, 14251; Kresse, G.; Furthmüller, J. *Comput. Mater. Sci*. **1996**, *6*, 15; Kresse, G.; Furthmüller, J. *Phys. Rev. B* **1996**, *54*, 11169.
(46) Vanderbilt, D. *Phys. Rev. B* **1990**, *41*, 7892.; Kresse, G.; Hafner, J. *J. Phys.: Condens. Matter* **1994**, *6*, 8245.
(47) Barrett, N. T.; Guillot, C.; Villette, B.; Treglia, G.; Legrand, B. *Surf. Sci*. **1991**, *251*, 717.; Klepeis, J. E. Terminello, L. J. *Phys. Rev. B* **1996**, *53*, 16035.
(48) Stauffer, L.; Mharchi, A.; Saintenoy, S.; Pirri, C.; Wetzel, P.; Bolmont, D.; Gewinner, G. *Phys. Rev. B* **1995**, *52*, 11932.; Swanston, D. M.; McLean, A. B.; McIlroy, D. N.; Heskett, D.; Ludeke, R.; Munekata, H.; Prietsch, M.; DiNardo, N. J. *Surf. Sci.* **1994**, *312*, 361.
(49) Kantorovich, L. N.; Holender, J. M.; Gillan, M. J. *Surf. Sci*. **1995**, *343*, 221.; Lindan, P. J. D.; Muscat, J.; Bates, S.; Harrison, N. M.; Gillan, M. *Faraday Discuss*. **1997**, *106*, 135.
(50) Korhonen, T.; Puska, M. J.; Nieminen, R. M. *Phys. Rev. B* **1995**, *51*, 9526.
(51) Polatoglou, H. M.; Methfessel, M.; Scheffler, M. *Phys. Rev. B* **1993**, *48*, 1877.
(52) Perdew, J. P.; Chevary, J. A.; Vosko, S. H.; Jackson, K. A.; Pederson, M. R.; Singh, D. J.; Fiolhas, C. *Phys. Rev. B*: *Condens. Matter* **1992**, *46*, 6671.
(53) Goniakowski, J.; Gillan, M. J. *Surf. Sci*. **1996**, *350*, 145.; de Leeuw, N. H.; Purton, J. A.; Parker, S. C.; Watson, G. W.; Kresse, G. *Surf. Sci*. **2000**, *452*, 9.
(54) Kittel, C. *Introduction to Solid State Physics*; John Wiley & Sons Inc.: New York, 1996.
(55) Monkhorst, H. J.; Pack, J. D. *Phys. Rev. B* **1976**, *13*, 5188.
(56) Methfessel, M.; Paxton, A. T. *Phys. Rev. B* **1989**, *40*, 3616.
(57) Wang, Y.; Wang, W.; Fan, K.-N.; Deng, J. *Surf. Sci*. **2001**, *490*, 125.
(58) Smith, J. R.; Banerjea, A. *Phys. Rev. Lett*. **1987**, *59*, 2451.
(59) Culbertson, R. J.; Feldman, L. C.; Silverman, P. J.; Boehm, H. *Phys. Rev. Lett*. **1981**, *47*, 657.
(60) Statiris, P.; Lu, H. C.; Gustafsson, T. *Phys. Rev. Lett*. **1994**, *72*, 3574.
(61) Foils, S. M.; Baskes, M. J.; Daw, M. S. *Phys. Rev. B* **1986**, *33*, 7983.
(62) Soares, E. A.; Leatherman, G. S.; Diehl, R. D.; Van Hove, M. A. *Surf. Sci*. **2000**, *468*, 129.
(63) de Leeuw, N. H.; Parker, S. C.; Catlow, C. R. A.; Price, G. D. *Am. Mineral*. **2000**, *85*, 1143.
(64) Haftel, M. I. *Phys. Rev. B* **2001**, *64*, 125415.
(65) Giesen, M.; Schulze Icking-Konert, G.; Ibach, H. *Phys. Rev. Lett*. **1998**, *80*, 552.; Giesen, M.; Ibach, H. *Phys. Rev. Lett*. **2000**, *85*, 469.; Morgenstern, K.; Rosenfeld, G.; Comsa, G.; Lægsgaard, E.; Besenbacher, F. *Phys. Rev. Lett*. **2000**, *85*, 468.; Hoogeman, M. S.; Klik, M. A. J.; van Gastel, R.; Frenken, J. W. M. *J. Phys. Condens. Matter* **1999**, *11*, 4349.